Thin Solid Films 689 (2019) 137457

Contents lists available at ScienceDirect

Thin Solid Films

journal homepage: www.elsevier.com/locate/tsf

Atomistic simulations of dipole tilt wall stability in thin films

Jun Xu[a,*], Shuozhi Xu[b], Irene J. Beyerlein[b,c]

[a] Department of Physics, University of California, Santa Barbara, Santa Barbara, CA 93106-9530, USA
[b] California NanoSystems Institute, University of California, Santa Barbara, Santa Barbara, CA 93106-6105, USA
[c] Department of Mechanical Engineering and Materials Department, University of California, Santa Barbara, Santa Barbara, CA 93106, USA

ARTICLE INFO

Keywords:
Dipole tilt wall
Copper thin films
Molecular statics

ABSTRACT

In this work, we use molecular statics to study the stability of a pair of symmetric dipole tilt walls in Cu thin films. Two geometric wall parameters, the dislocation spacing and wall separation distance, are varied in the calculations. We find that even closely spaced dipole walls can be stabilized in a thin film under no applied strain, and with this insight, develop a stability map that identifies the regime of maximum dislocation spacing and minimum wall separation for which dipole walls can reside in the film. In addition, we show that a critical in-plane tensile strain exists that can destabilize the dipole walls and transition the film to a wall-free state. The simulations reveal that the wall recovery process occurs by sequentially annihilating alternating pairs of dipole dislocations rather than sudden, simultaneous annihilation of an entire wall. Dipole wall stability is rationalized based on a substantial enhancement in the Peierls barrier of the wall dislocations due to the reorientation of the lattice between the walls and narrowing of their intrinsic stacking faults, two effects that have atomic-scale origins.

1. Introduction

The deformation of metallic thin films subject to an applied strain or residual strains is accommodated by the formation and glide of dislocations. In the early stages of straining from a nearly defect free state, dislocation glide meets little resistance [1]. After moderate amounts of strain (0.1–1), the density of dislocations can increase by two to three orders of magnitude [2,3]. Accumulated dislocations tend not to be distributed uniformly but assembled into patterns [4–6]. Over the years, the origins of these sub-boundaries have garnered considerable attention due to the marked effect on the electronic, magnetic, and structural properties of materials. For example, sub-boundary mobilities have been shown to be positively correlated with recrystallization rates in polycrystals [7]. The stress fields generated from sub-boundaries can interact with moving dislocations, hindering their glide, and limiting plasticity. Dislocations within these sub-boundaries can also directly react with mobile lattice dislocations, severely hampering the latter from gliding across the former [8] and encouraging dislocation pile ups and hence generation of stress concentrations [9]. Because the length scales of the gliding dislocations are comparable to that of the constitute dislocations in the sub-boundaries, the ability for dislocations to transfer slip across the boundaries depend sensitively on their local, atomic-scale defect structures [10].

The length scales and morphologies of the dislocation patterns have been studied most extensively in deformed materials postmortem via microscopy [11]. The propensity for patterning increases as the amount of deformation and rate of deformation decreases, resulting in loose tangles in shock [12], well defined sub-boundaries after rolling [13], and increasing sub-boundary dislocation density with creep deformation [14]. To understand their development during deformation, two-dimensional (2D)and three-dimensional (3D)dislocation dynamics simulations based on linear elasticity theory have been employed. They have predicted self-organization of dislocations under a continually rising externally applied strain into linear pileups [15] and sub-boundaries in the form of 2D dipole walls [16] and 3D bands [17].

One type of dislocation sub-boundary prevalent in thin films are tilt dislocation walls [18,19]. They can be described as an array of edge dislocations with their dislocation lines on separate but parallel planes. The lattices on either side of the wall are tilted in equal amounts in opposing senses [20]. The ability of moving dislocations to penetrate a tilt wall depends sensitively on the wall misorientation angle θ and the wall frequency (or equivalently wall spacing). Unlike general sub-boundaries, tilt walls with low θ contain sparsely stacked dislocations pose relatively little resistance to moving dislocations by altering their slip plane without directly interacting with any of the constituent dislocations in the wall [21]. Toward understanding their development is

* Corresponding author.
E-mail address: junxu@ucsb.edu (J. Xu).

https://doi.org/10.1016/j.tsf.2019.137457
Received 16 May 2019; Received in revised form 22 July 2019; Accepted 28 July 2019
Available online 06 August 2019
0040-6090/

the stability of these walls under no applied deformation as well as under a critical applied deformation to remove them. Yet most analytical studies [22], continuum-based modeling [23], and atomistic simulations [24] treat tilt dislocation walls in an infinite body, instead of in a thin film.

In this work, we use molecular statics (MS) to determine the stability of dipole tilt walls in copper (Cu) thin films in both undeformed and deformed states. The effects of two key geometric parameters describing the dipole wall pair, the wall spacing and internal wall dislocation spacing, on their atomic defect structure and stability are investigated. A regime of stable dipole wall configurations is identified and linked to the increased resistance to dislocation motion due to lattice misorientation and narrowing of the associated intrinsic stacking faults (ISF). Last we show that a critical in plane tensile strain exists that eliminates the dipole wall and the process of dipole wall elimination occurs by a sequential process rather than a simultaneous one.

2. Materials and methods

We select Cu as a model material with a face-centered cubic (FCC) crystal structure. As dislocations in FCC metals belong to the {111}⟨110⟩ slip system, tilt dislocation walls can be described by a vertical array of edge dislocations belonging to this slip system with the tilt axis lying along ⟨112⟩. Fig. 1 illustrates the simulation cell containing two finite-length dipole dislocation walls in a thin film. The crystallographic orientations are $x[\bar{1}10]$, $y[111]$, and $z[11\bar{2}]$, with the y direction serving as the normal to the film. To model a thin film, periodic boundary conditions are applied along the x and z directions, while the top and bottom surfaces of the film, the y-boundaries, are traction-free.

Thin film models are designed to examine the effects of two wall parameters: the initial dipole wall separation h_{x0} and dislocation spacing in each wall d, on the stability of the dipole walls under zero stress and in-plane tensile strain. Unless stated otherwise, the film thickness $L_y = 50.8$ nm, and the two in-plane dimensions in the x and z directions, respectively, $L_x = 122.9$ nm and $L_z = 0.9$ nm. In selected cases, L_x and L_y will be varied to assess their influences. The distance between the top dislocation in each wall and the cell upper boundary, $h' = 1.59$ nm, as well as the distance between the bottom dislocation in each wall and the cell lower boundary, $h'' = 1.59$ nm are fixed in every case. The film thickness L_y is related to the number of dislocations N in each wall and d according to

$$L_y = h' + h'' + (N-1)d \tag{1}$$

Each edge dislocation in the wall is created by displacing all atoms by (u_x, u_y) following the corresponding isotropic elastic displacement fields [25], i.e.,

$$u_x(\bar{x},\bar{y}) = \frac{b}{2\pi}\left[\tan^{-1}\left(\frac{\bar{y}}{\bar{x}}\right) + \frac{\bar{x}\bar{y}}{1-\nu}(\bar{x}^2+\bar{y}^2)\right] \tag{2}$$

$$u_y(\bar{x},\bar{y}) = \frac{b}{2\pi}\left[\frac{1-2\nu}{4(1-\nu)}\log(\bar{x}^2+\bar{y}^2) + \frac{\bar{x}^2+\bar{y}^2}{4(1-\nu)}(\bar{x}^2+\bar{y}^2)\right] \tag{3}$$

where b is the magnitude of the Burgers vector of an edge dislocation, ν is the Poisson's ratio, and $(\bar{x}, \bar{y})$ is the relative position of each atom with respect to the dislocation core center along the x and y axes, respectively.

All MS simulations in this work are carried out by LAMMPS [26]. The interatomic interactions between Cu atoms are provided by an embedded-atom method (EAM) potential [27] because it has proven to describe well many dislocation-related material properties [28,29]. The lattice parameter for Cu is $a_0 = 0.3615$ nm, and each model contains 460,800 atoms. As such, $b = a_0/\sqrt{2} = 0.2556$ nm. Atomic structures are visualized by OVITO [30] and the adaptive common neighbor analysis (a-CNA) [31] is used to identify dislocations.

Once the two dislocation walls are created, MS simulations with the conjugate gradient algorithm are carried out and are terminated when one of the following two criteria is satisfied: (i) the change in energy between successive iterations divided by the most recent energy magnitude is less than or equal to 10^{-9} and (ii) the length of the global force vector for all atoms is less than or equal to 10^{-9} eV/Å. During the energy minimization, all edge dislocations dissociate into two Shockley partials that glide apart on the (111) planes. An ISF forms between them. The distance between the centers of the two bounding Shockley partials is defined as the ISF width [32].

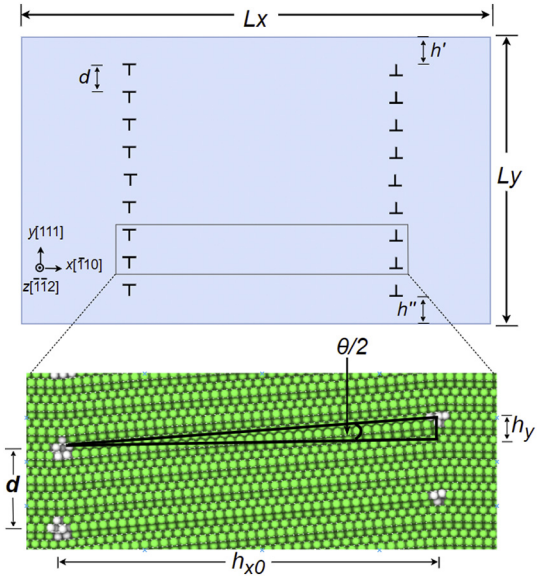

Fig. 1. An illustration of a Cu thin film containing two vertical dislocation walls of opposite sign. Fixed geometric parameters include depth of the model $L_z = 0.9$ nm and $h' = h'' = 1.59$ nm. Different models are considered in which L_x, L_y, h_{x0}, and d vary. The zoomed out snapshot shows the atomic structures around two dislocation dipoles prior to the energy minimization. Atoms are colored by a-CNA [31]: green and white corresponds to FCC and disordered local lattice structures, respectively.

3. Results and discussion

3.1. Wall stability under zero stress

In this section, we study the wall stability under zero stress as a function of the vertical dislocation spacing d and the initial wall separation h_{x0}. L_x and L_y are also varied in selected cases.

As a reference, we first consider a single dislocation dipole of two oppositely signed edge dislocations lying in the same plane. When the system is relaxed the dislocations may move toward one another and annihilate. The reason is well known. The interaction force between these two dislocations is attractive. This force can be approximated using linear elastic dislocation theory. For two edge dislocations of opposite sign separated by h_{x0} on the same plane, the attractive force per unit length is [1]

$$F_{x0} = \frac{\mu b^2}{2\pi h_{x0}(1-\nu)} \tag{4}$$

where μ is the isotropic shear modulus. Let the horizontal wall spacing $h_{x0} = 10$ nm. Using the Voigt average to estimate the isotropic equivalent moduli for Cu, $\mu = 41.16$ GPa and $\nu = 0.34$, we obtain $F_{x0} = 64.8$ mN/m for the interaction force between these two dislocations. The only resistance to this force is the intrinsic material resistance, the Peierls stress [33]. Previously, the same EAM potential calculates the Peierls stress for a single, isolated dislocation to be $\tau_P = 2.5$ MPa [34]. The corresponding resisting force per unit length $\tau_P b = 0.639$ mN/m is two orders of magnitude below F_{x0}. With relatively little resistance, the dislocations can easily glide on their shared

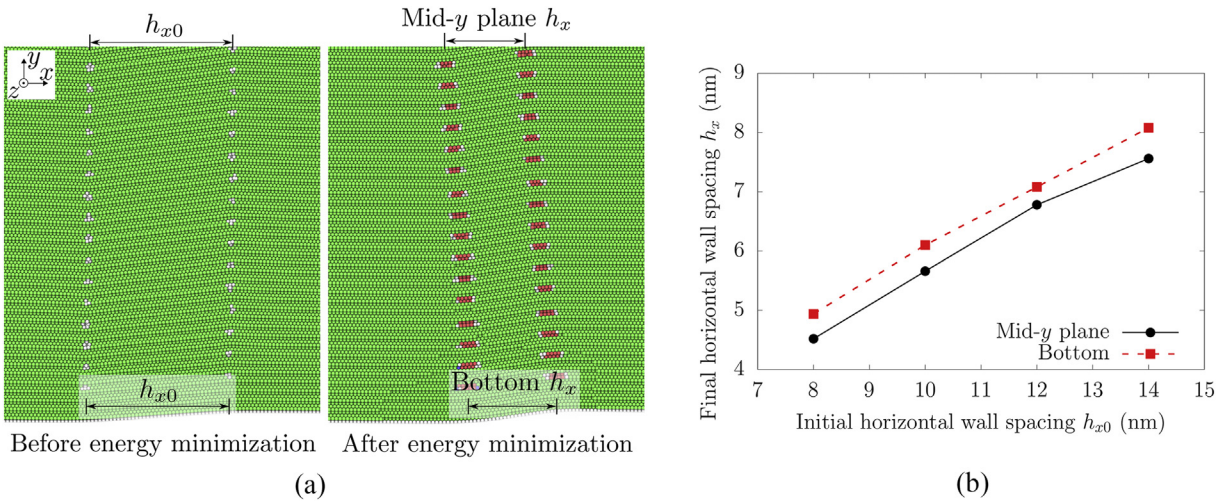

Fig. 2. (a) Atomic structures of the dipole tilt wall before and after energy minimization. L_y = 50.8 nm, h_{x0} = 10 nm, and d = 1.5 nm. Atoms are colored by a-CNA [31]: green, red, blue, and white corresponds to FCC, hexagonal close-packed, body-centered cubic, and disordered local lattice structures, respectively. (b) Final horizontal wall spacing h_x after energy minimization in cases of different initial horizontal wall spacing h_{x0}. Values of h_x and h_{x0} shown here are averaged over those in different models with different vertical dislocation spacing d.

glide plane and annihilate. Alternatively, for this situation, we can use Eq. 4 to determine the critical wall separation above which the dipole walls are stable, i.e., $F_{x0} \leq \tau_P b$; the critical separation is found to be 1014.08 nm, an extremely large value.

Next, we consider a pair of dipole tilt walls within the thin film. The two walls are identical, sharing the same tilt axis and same dislocation spacing d. They only differ in the sign of the dislocations in the wall. The wall on the right contains positive dislocations and the one on the left negative dislocations. As before, the initial wall separation is close, h_{x0} = 10 nm, so the walls should be strongly interacting. We first consider walls with a relatively large dislocation spacing of d = 7.94 nm, more than 30 times that of b. When allowing the system to relax, the dislocations in the two walls glide toward one another under the attractive interaction forces between their oppositely signed dislocations and annihilate. The dipole walls are not stable under zero stress.

More cases are simulated involving a pair of walls with even finer spacing d but the same separation h_{x0} = 10 nm. For values of $d > 3.21$ nm, the walls glide toward another and annihilate. When d = 3.21 nm, however, the walls glide toward one another and stop with a final separation of h_x. Fig. 2a shows the stable configuration. The mid-plane separation is smaller compared to the wall separation near the surface (Fig. 2b). The stress state locally at the surface opposes the glide of dislocations toward one another. The difference is not significant. The main finding is that we have identified a critical spacing, d_c = 3.21 nm, at and below which the dipole walls can be stabilized.

The critical d_c is far below the total thickness of the film to be affected by it. However, to be certain, we examined the effects of film thickness L_y on d_c, by repeating the calculations while setting L_y to 40.4 nm and 59.7 nm, respectively. The critical d_c did not change.

In present simulations, a condition evidently is reached in which the critical stress to move the dislocation constituting the walls, the Peierls stress, has increased to surpass the attractive interaction stress between them. The elastic stress fields between two interacting dipole tilt walls have been studied analytically using linear elastic continuum dislocation mechanics [35,36]. On this basis, this pair of walls would be expected to annihilate since the calculated attractive force per unit length exceeds that associated with the Peierls stress $\tau_P b$ = 0.639 mN/m. However, these walls do not annihilate, suggesting that attainment of a zero-stress stable dipole wall configuration must then have atomic-scale origins captured in the atomistic calculation but not in the continuum mechanics model. In the latter model, the dislocations are undissociated and each dislocation dipole lies on the same plane. In atomistic simulations, however, the lattice between the walls has rotated and is misoriented across each wall. Further, the dislocations in the walls are dissociated.

To understand the origin of the wall stability, we first consider lattice misorientations on the interaction stress. The walls have caused the slip planes between the walls to tilt, which changes the dipole interaction force per unit length in Eq. 4 to [1]:

$$F_x = \frac{h_{x0}(h_{x0}^2 - h_y^2)}{(h_{x0}^2 + h_y^2)^2} \cdot \frac{\mu b^2}{2\pi(1-\nu)} \tag{5}$$

where h_y is the vertical distance between the two dislocations in the same dipole due to the plane tilt, as illustrated in Fig. 1. This interaction force considers a single dipole, so the force fields by the other dislocations in the wall are not included; however, these would have a relatively small contribution compared to the nearest oppositely signed dislocation. We calculate the interaction force per unit length between the two walls using Eq. 5, where h_x is substituted for h_{x0}. At d = 3.21 nm, h_y = 0.34 nm on the mid-y plane, and hence $F_x = 0.9967 F_{x0}$. This value of F_x is slightly lower than F_{x0}, yet still much larger than $\tau_P b$. Therefore, the change in the interaction force due to the misorientation cannot explain stabilization of the dipole wall.

In light of the foregoing analysis, stabilization can be perceived as a result of an increase in the Peierls stress of the constituent dislocations when lying in wall compared to when each is in isolation. Two atomic-scale changes are readily apparent. First, within the wall, at the dislocation site, the glide plane abruptly changes orientation, severely hindering glide, and second, the dislocation core has been altered. We study next the effect of d on both lattice misorientation angle and ISF width for the dipole wall configuration.

The dipole tilt walls cause the lattice in between them to tilt, hindering the dislocations to glide. In the case of an isolated, infinitely long wall with a uniform vertical dislocation spacing d, the misorientation angle θ is

$$\theta = 2\arcsin\left(\frac{b}{2d}\right) \tag{6}$$

For the stabilized dipole walls, θ can be directly measured based on the energy minimized atomistic structures by

$$\theta = 2\arctan\left(\frac{h_y}{h_x}\right) \tag{7}$$

For the dipole wall, the misorientation angle will deviate from that

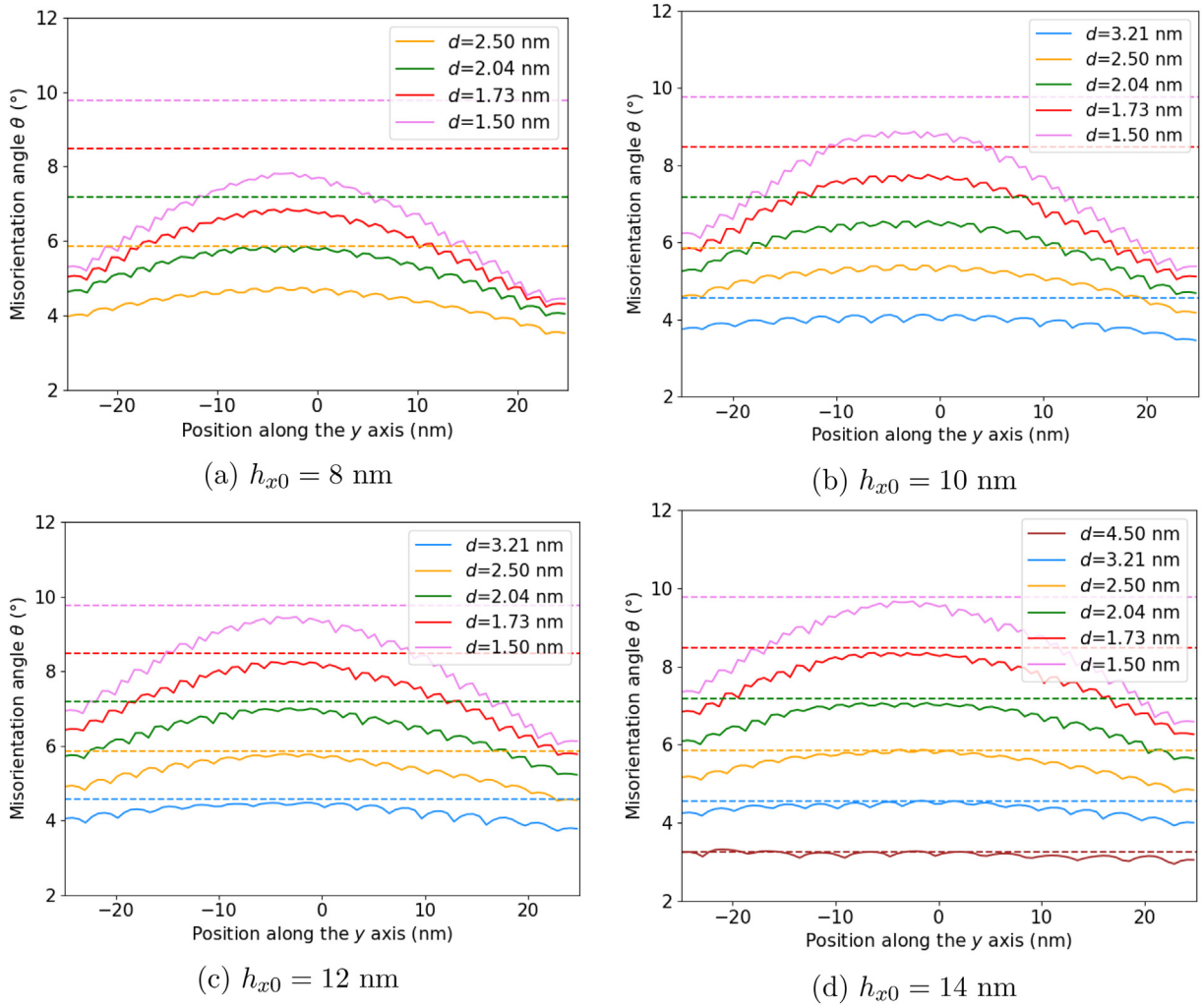

Fig. 3. The misorientation angle θ along the y axis based on Eq. 7, measured after the energy minimization in models with different initial horizontal wall spacing h_{x0} and uniform vertical dislocation spacing d. The predictions of θ based on Eq. 6, denoted by horizontal dashed lines, are also shown for references.

of a single wall, provided the two walls are sufficiently close. Using Eq. 7 the through-thickness variation of θ are calculated for different values of h_{x0} and d for which a stable dipole wall configuration is achieved. Fig. 3 shows the calculated θ after the configuration has stabilized. For comparison, also shown is the corresponding misorientation angle predicted by Eq. 6 for one wall with the same d. As seen earlier, the effect of the free surfaces at the top and bottom of the film is to locally increase the dipole wall separation from the center, leading to a lower misorientation angle at the top and bottom film surfaces than that at the center of the film. The misorientation angles of the two walls rotate the lattice in between them in the same sense. When the walls are initially closely spaced, h_{x0} = 8 nm, the misorientation angle of the lattice in-between is reduced from that of a single wall for all d. For instance, when h_{x0} = 8 nm and d = 1.5 nm, the measured θ on the mid-y plane is about 8° while the theoretical prediction for a single wall is about 10°. The analysis also finds that for a wall separation of almost double, h_{x0} = 14 nm, the misorientation angle measured in the center of the film is almost the same as that for a single wall. Using $F_{x0} \leq \tau_P b$ as a condition for stability, along with Eqs. 5 and 7, we can estimate the Peierls stress for every stabilized wall configuration. This analysis implies that the Peierls stress in the wall must have ranged from 181.09 to 316.9 MPa.

In FCC metals, the Peierls stress is strongly influenced by the ISF width, w. Wider ISFs generally have lower resistance to glide than narrower ones. Prior density functional theory calculations in Al showed that, compared with a dissociated screw dislocation ($w = 3.81b$), the Peierls stress of an undissociated screw dislocation ($w = b$) is much higher by approximately two orders of magnitude [37]. Qualitatively, a similar boost in the Peierls stress can be expected in Cu, since it has the same crystal structure and bonding type as Al. Fig. 4 shows the average ISF width of a dislocation in the dipole wall. Each dislocation has dissociated into two Shockley partials, with equal edge components and oppositely signed screw dislocations. As d decreases,

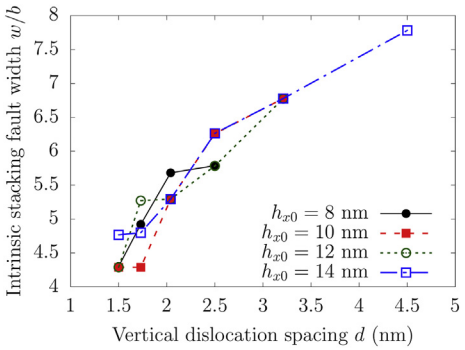

Fig. 4. ISF width w on the mid-y plane in simulation cells with different initial horizontal wall spacing h_{x0} and uniform vertical dislocation spacing d. For an isolated edge dislocation, $w = 10.57b$ [28].

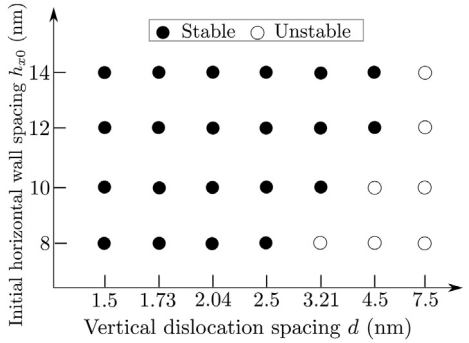

Fig. 5. Map indicating whether the dislocation walls are stable for a specific initial horizontal wall spacing h_{x0} and uniform vertical dislocation spacing d.

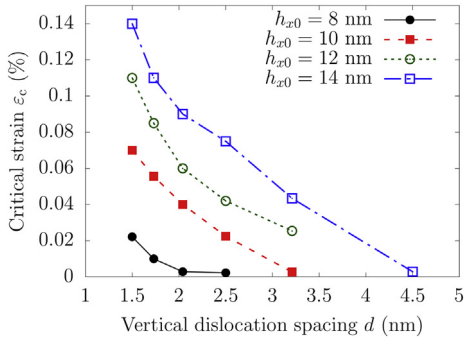

Fig. 6. Critical strains for the dislocation dipole annihilation ε_c in models with different initial horizontal wall spacing h_{x0} and uniform vertical dislocation spacing d.

the attraction force between the neighboring screw components increases, causing the wall w to narrow. When $d = 3.21$ nm, for instance, $w = 6.78b$ on the mid-y plane, which is much smaller than $10.57b$ [38]. Narrowing of w as d decreases could significantly raise the Peierls stress, which may surpass the elastic attraction between dislocations.

It has, thus far, been shown that with smaller d a dipole wall can be stabilized provided that the wall spacing d is below d_c, arguably when the slip plane misorientation across the wall and the widths of the ISFs have become sufficiently narrow to stall motion of the wall dislocations. According to Eq. 5 misorientation depends on the wall separation distance, implying that d_c would depend on how far they are separated. To investigate the effects of the initial horizontal wall spacing h_{x0} on wall stability, we consider small wall separations that tend to lower the wall misorientation angle compared to that of an isolated wall (8 nm, 10 nm, and 12 nm) and a sufficiently large wall separation when it is close to it (14 nm). Recall from earlier analysis, when $h_{x0} = 10$ nm, d_c is 3.21 nm. Comparatively when h_{x0} increases from 8 nm and 12 nm, to 14 nm, d_c increases from 2.5 nm and 3.21 nm to 4.5 nm. With this insight, a region in h_{x0}-d space can be envisioned, wherein a dipole wall can be stabilized. Fig. 5 shows a h_{x0}-d map for the Cu film arising from these calculations. A region associated with large h_{x0} and small d corresponds to dipole wall stability. To assess the influence of the length of the model along the x direction, L_x, we repeat the calculations with larger L_x of 180 nm and 265 nm, respectively, and find that the stability map remains unchanged from $L_x = 122.9$ nm.

3.2. Wall stability under tensile loading

Next we examine dipole wall stability under mechanical deformation. In MS simulations, thin films containing stable dipole wall configurations are strained until a threshold strain is reached at which the walls are able to glide together and annihilate. An in-plane tensile strain would tend to reorient the lattice back to its original planar orientation, reducing the barrier to wall glide, enabling the dislocations in the dipole wall to move toward one another under an attractive force. On this basis it would be anticipated that the higher the lattice misorientation, the more resistant the dipole configurations to recovery. The force on the dislocations from the strain applied in the loading direction is minimal since the tilts are relatively small. For example, for a tilt angle of 8°, the Schmid factor on the central dislocation is 0.14. Thus, in this case, the key effect provided by the applied deformation is to reduce the impediment to wall destabilization and recovery of a perfect film.

In the calculations, after the system energy is minimized and the dipole walls stabilized, an incremental tensile strain is applied to the thin film along the x direction. After every increment in true strain (0.001%), the total system energy is minimized. Fig. 6 shows the variation in the critical strain ε_c for a broad range of h_{x0} and d. The most stable walls are those that develop the highest misorientations, which are the widely separated walls (large h_{x0}) and those with fine dislocation spacing (small d). The interesting aspect is the strong sensitivity to these variables. For $d = 2.04$ nm, nearly doubling the separation from 8 nm to 14 nm leads to a ten-fold increase in ε_c. Likewise, for $h_{x0} = 10$ nm, a change in d from 1.5 nm to 3.21 nm dramatically decreases ε_c from 0.07% to 0.003%.

These critical strains are governed by the process of dislocation annihilation. Rather than gliding uniformly toward each other on their respective habit planes and annihilating simultaneously, the dislocations in the walls annihilate through sequence of events. Fig. 7 shows a few snapshots of the annihilation process in consecutive stages. In Fig. 7(b), the walls first move together simultaneously and stop. Next dislocation dipoles on alternating planes draw closer and annihilate (e.g., dislocation pairs C/D and G/H in Fig. 7). The remaining configuration is a dipole tilt wall with double dislocation spacing, as shown in Fig. 7(c). Next, dislocations in alternating planes of these dipole walls glide toward one another and annihilate, leaving a dipole pair of walls those spacing doubles that of the previous walls or quadruples that of the original walls, as shown in Fig. 7(d). This pattern occurs repeatedly until all dislocations in the dipole walls annihilate.

Fig. 8 illustrates the process to elucidate the underlying mechanisms. The key maneuver in the wall recovery process is the formation of a zig-zag configuration. Under deformation the tilt walls draw closer (Fig. 8(a)) until at some point they form a zig-zag pattern (Fig. 8(b)), wherein the dislocations on alternating planes draw closer while those on every other plane glide apart. This alternative configuration zig-zag configuration is another well known stable configuration for a pair of dipole dislocations on parallel but separate planes [39]. By creating the zig-zag pattern, the planes with the more closely spaced dislocation dipoles are able to annihilate. The remaining dislocations lie in a pair of walls with large dislocation spacing and hence lower tilt angles, as shown in Fig. 8(c). These two walls subsequently and simultaneously draw closer, assuming a zig-zag arrangement again (Fig. 8(d)) and enabling the more closely spaced dislocation dipoles to annihilate. At the critical strain ε_c, all dislocations are annihilated.

4. Conclusions

In this work, atomistic simulations are conducted to study the stability of dipole tilt walls in Cu thin films. The effects of the initial wall separation h_{x0} and wall dislocation spacing d are investigated. For thin films under zero stress, we show that there exists a critical dislocation spacing below which even closely spaced dipole walls can be stabilized. Dipole wall stability is explained by an increased resistance to dislocation motion due to lattice misorientation and narrowing of the associatedISFs. A measure of dipole wall stability is identified as a critical in-plane tensile strain above which the dipole walls become destabilized and annihilate one another, leaving a wall-free film. The more stable wall configurations (or higher critical tensile strains) are associated with finer dislocation wall spacing and wider wall separations. Subject to a tensile loading, it is revealed that the process of

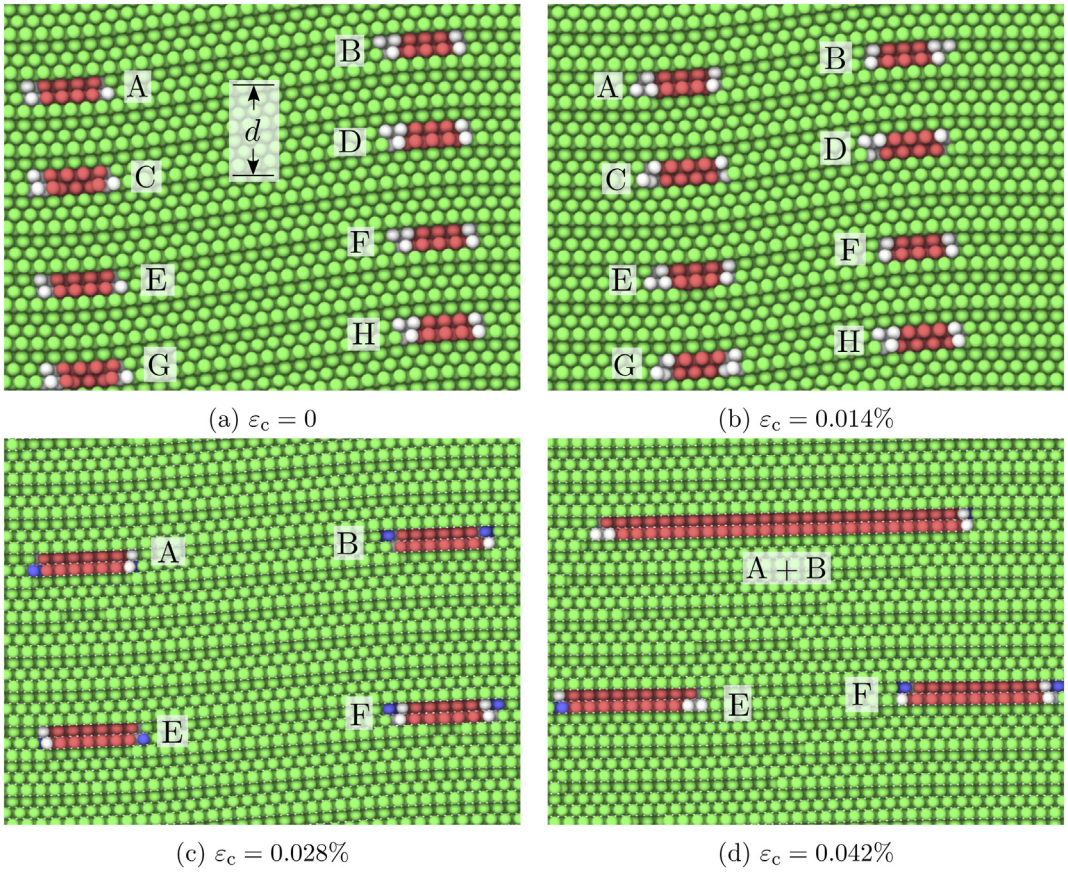

Fig. 7. Atomic structures of the annihilation of selected dislocation dipoles subject to the tensile loading. h_{x0} = 10 nm and d = 1.5 nm. Eight dislocations taken near the mid-y plane are indexed as A, B, …, H. Atoms are colored in the same way as in Fig. 2a.

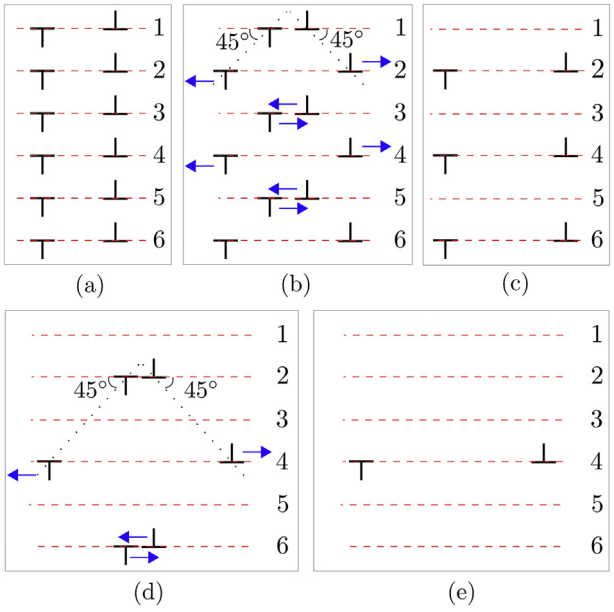

Fig. 8. An illustration that shows the sequence of dislocation annihilation during the tensile loading. In (b) and (d), every other dislocation dipole is drawn closer or pushed further away, forming a 45° angle between the two vertically adjacent dislocations in the same wall.

dipole wall elimination occurs by a sequential, multi-step process rather than a single, simultaneous one. Alternating dislocation dipoles annihilate first, leaving the dipole walls with a larger dislocation spacing and hence less stable under the ensuing tensile strain. The process continues until the entire wall has been removed.

Acknowledgements

The work of SX was supported in part by the Elings Prize Fellowship in Science offered by the California NanoSystems Institute on the UC Santa Barbara campus. IJB acknowledges financial support from the National Science Foundation Designing Materials to Revolutionize and Engineer our Future (DMREF) program (NSF CMMI-1729887). Use was made of computational facilities purchased with funds from the National Science Foundation (CNS-1725797) and administered by the Center for Scientific Computing (CSC). The CSC is supported by the California NanoSystems Institute and the Materials Research Science and Engineering Center (MRSEC; NSF DMR 1720256) at UC Santa Barbara. This work used the Extreme Science and Engineering Discovery Environment (XSEDE), which is supported by National Science Foundation grant number ACI-1053575.

References

[1] D. Hull, D.J. Bacon, Introduction to Dislocations, 5th ed, Butterworth-Heinemann, 2011.
[2] S.Z. Chavoshi, S. Xu, Nanoindentation/scratching at finite temperatures: Insights from atomistic-based modeling, Prog. Mater. Sci. 100 (2019) 1–20.
[3] S. Xu, X. Chen, Modeling dislocations and heat conduction in crystalline materials: atomistic/continuum coupling approaches, Int. Mater. Rev. 64 (2019) 407–438.
[4] D.L. Holt, Dislocation cell formation in metals, J. Appl. Phys. 41 (1970) 3197–3201.
[5] D. Kuhlmann-Wilsdorf, N.R. Comins, Dislocation cell formation and work hardening in the unidirectional glide of f. c.c. metals I: Basic theoretical analysis of cell walls parallel to the primary glide plane in early stage II, Mater. Sci. Eng. 60 (1983) 7–24.
[6] S. Xu, Modelling plastic deformation of nano/submicron-sized tungsten pillars under compression: A coarse-grained atomistic approach, Int. J. Multiscale Comput. Eng. 16 (2018) 367–376.

[7] L. Germain, D. Kratsch, M. Salib, N. Gey, Identification of sub-grains and low angle boundaries beyond the angular resolution of EBSD maps, Mater. Charact. 98 (2014) 66–72.
[8] S. Xu, L. Xiong, Y. Chen, D.L. McDowell, Sequential slip transfer of mixed-character dislocations across Σ3 coherent twin boundary in FCC metals: a concurrent atomistic-continuum study, npj Comput. Mater. 2 (2016) 15016.
[9] X. Zhang, J. Han, J.J. Plombon, A.P. Sutton, D.J. Srolovitz, J.J. Boland, Nanocrystalline copper films are never flat, Science 357 (2017) 397–400.
[10] T. Shimokawa, T. Kinari, S. Shintaku, Interaction mechanism between edge dislocations and asymmetrical tilt grain boundaries investigated via quasicontinuum simulations, Phys. Rev. B 75 (2007) 144108.
[11] M.A. Crimp, Scanning electron microscopy imaging of dislocations in bulk materials, using electron channeling contrast, Microsc. Res. Tech. 69 (2006) 374–381.
[12] F. Cao, I.J. Beyerlein, F.L. Addessio, B.H. Sencer, C.P. Trujillo, E.K. Cerreta, G.T.G. Iii, Orientation dependence of shock-induced twinning and substructures in a copper bicrystal, Acta Mater. 58 (2010) 549–559.
[13] D.A. Hughes, N. Hansen, The microstructural origin of work hardening stages, Acta Mater. 148 (2018) 374–383.
[14] M. Ben Saada, N. Gey, B. Beausir, X. Iltis, H. Mansour, N. Maloufi, Sub-boundaries induced by dislocational creep in uranium dioxide analyzed by advanced diffraction and channeling electron microscopy, Mater. Charact. 133 (2017) 112–121.
[15] A. Roy, R.H.J. Peerlings, M.G.D. Geers, Y. Kasyanyuk, Continuum modeling of dislocation interactions: Why discreteness matters? Mater. Sci. Eng. A 486 (2008) 653–661.
[16] C. Zhou, C. Reichhardt, C.J. Olson Reichhardt, I.J. Beyerlein, Dynamic phases, pinning, and pattern formation for driven dislocation assemblies, Sci. Rep. 5 (2015) 8000.
[17] Z.Q. Wang, I.J. Beyerlein, R. LeSar, Slip band formation and mobile dislocation density generation in high rate deformation of single fcc crystals, Philos. Mag. 88 (2008) 1321–1343.
[18] T. Schober, R.W. Balluffi, Dislocation sub-boundary arrays in oriented thin-film bicrystals of gold, Philos. Mag. A 20 (1969) 511–518.
[19] R.A. Wind, M.J. Murtagh, F. Mei, Y. Wang, M.A. Hines, S.L. Sass, Fabrication of nanoperiodic surface structures by controlled etching of dislocations in bicrystals, Appl. Phys. Lett. 78 (2001) 2205–2207.
[20] R. Wirth, Focused ion Beam (FIB): A novel technology for advanced application of micro- and nanoanalysis in geosciences and applied mineralogy, Eur. J. Mineral. 16 (2004) 863–876.
[21] Y. Gao, Z. Jin, Interactions between lattice dislocation and Lomer-type low-angle grain boundary in nickel, Comput. Mater. Sci. 138 (2017) 225–235.
[22] E. Smith, The distribution of dislocations in two pile-ups, arranged one above the other, Int. J. Eng. Sci. 4 (1966) 451–461.
[23] B. Liu, D. Raabe, P. Eisenlohr, F. Roters, A. Arsenlis, G. Hommes, Dislocation interactions and low-angle grain boundary strengthening, Acta Mater. 59 (2011) 7125–7134.
[24] Y. Gao, Z. Jin, Interaction between lattice dislocations and low-angle grain boundaries in Ni via molecular dynamics simulations, Mol. Simul. 43 (2017) 1172–1178.
[25] S. Xu, R. Che, L. Xiong, Y. Chen, D.L. McDowell, A quasistatic implementation of the concurrent atomistic-continuum method for FCC crystals, Int. J. Plast. 72 (2015) 91–126.
[26] S. Plimpton, Fast parallel algorithms for short-range molecular dynamics, J. Comput. Phys. 117 (1995) 1–19.
[27] Y. Mishin, M.J. Mehl, D.A. Papaconstantopoulos, A.F. Voter, J.D. Kress, Structural stability and lattice defects in copper: *Ab initio*, tight-binding, and embedded-atom calculations, Phys. Rev. B 63 (2001) 224106.
[28] Y. Su, S. Xu, On the role of initial void geometry in plastic deformation of metallic thin films: a molecular dynamics study, Mater. Sci. Eng. A 678 (2016) 153–164.
[29] S. Xu, Y. Su, D. Chen, L. Li, Plastic deformation of Cu single crystals containing an elliptic cylindrical void, Mater. Lett. 193 (2017) 283–287.
[30] A. Stukowski, Visualization and analysis of atomistic simulation data with OVITO—the Open Visualization Tool, Model. Simul. Mater. Sci. Eng. 18 (2010) 015012.
[31] A. Stukowski, Structure identification methods for atomistic simulations of crystalline materials, Model. Simul. Mater. Sci. Eng. 20 (2012) 045021.
[32] S. Xu, J.R. Mianroodi, A. Hunter, I.J. Beyerlein, B. Svendsen, Phase-field-based calculations of the disregistry fields of static extended dislocations in FCC metals, Philos. Mag. 99 (2019) 1400–1428.
[33] R. Peierls, The size of a dislocation, Proc. Phys. Soc. 52 (1940) 34.
[34] S. Xu, L. Xiong, Y. Chen, D.L. McDowell, An analysis of key characteristics of the frank-read source process in FCC metals, J. Mech. Phys. Solids 96 (2016) 460–476.
[35] T.R. Duncan, D. Kuhlmann-Wilsdorf, The stress fields of dislocation tilt boundaries in anisotropic cubic and diamond-type crystals, Phys. Stat. Sol. 18 (1966) 231–239 (b).
[36] R. Sedláček, M. Hecker, Stress fields of tilted dislocation walls, Comput. Mater. Sci. 11 (1998) 270–276.
[37] I. Shin, E.A. Carter, Possible origin of the discrepancy in Peierls stresses of fcc metals: first-principles simulations of dislocation mobility in aluminum, Phys. Rev. B 88 (2013) 064106.
[38] S. Xu, J. Rigelesaiyin, L. Xiong, Y. Chen, D.L. McDowell, Generalized continua concepts in coarse-graining atomistic simulations, in: H. Altenbach, J. Pouget, M. Rousseau, B. Collet, T. Michelitsch (Eds.), Generalized Models and Non-classical Approaches in Complex Materials 2, Advanced Structured Materials, Springer, Cham, 2018, pp. 237–260 https://link.springer.com/chapter/10.1007/978-3-319-77504-3_12.
[39] P.M. Anderson, J.P. Hirth, J. Lothe, Theory of Dislocations, 3 ed., Cambridge University Press, Cambridge, 2017.